Inverse model-based characterization of green roof thermal performance

P Gunn[1], H B Gunay[2], P J Van Geel[3]
Carleton University, 1125 Colonel By Drive, Ottawa, ON, K1S 5B6, Canada
[1]petergunn@cmail.carleton.ca, [2]burakgunay@cunet.carleton.ca, [3]paulvangeel@cunet.carleton.ca

Abstract

Modelling green roof physics has mainly consisted of developing complex numerical models of fine spatial discretization to simulate physical processes that occur between the many surfaces and materials that define the green roof system. However, a recent review of these models points out that (1) increasing model complexity may not necessarily translate into better predictability of key thermal performance metrics of interest (e.g., interior temperature), and (2) researchers and practitioners should consider developing parsimonious models which can predict processes that are more representative of green roof thermal performance. In this paper, we implement a resistor-capacitor (RC) model to characterize the thermal properties of the canopy and substrate of the green roof using an inverse modelling approach. The calibrated model is then evaluated based on its ability to predict hourly heat flux through the structural component of the green roof. Our results demonstrate a maximum root-mean-squared error of 0.84 W/m^2 for hourly heat flux across five separate months: May through September 2016. Reductions in total monthly heat exchange were better predicted during May and September when a large fraction of heat exchange was heat loss through the roof.

Introduction

Green roofs have been a promising alternative to conventional rooftop materials for realigning urbanized areas with the natural environment (Francis and Lorimer 2011). A green roof typically consists of a roofing membrane, drainage layer, geotextile filter, growth substrate, and vegetation that is carefully selected for resiliency against regional climate (Boafo et al. 2017). Benefits of green roofs have been quantified in recent years, including stormwater retention (Talebi et al. 2019), urban heat island mitigation (Santamouris 2014), and building energy use reduction (Susca 2019), among others. Indeed, a considerable amount of intellectual capital has been invested in understanding how green roofs diminish heat flux through roof envelopes, with many studies concluding that this thermal benefit is most pronounced during summer, when the dominant cooling mechanism is evapotranspiration (Saadatian et al. 2013).

Despite being the primary cooling process, evapotranspiration – the dissipation of latent energy that occurs when foliage converts soil moisture into water vapour for release through plant stomata – represents just one of the numerous energy exchanges that occur in green roof systems: radiative exchange, wind-driven convection, moisture-dependent conduction, shading, and heat storage all contribute to the overall thermal performance of green roofs. These processes have been represented in physics-based models that have been incorporated into building energy simulation (BES) tools like EnergyPlus such as the model by Sailor (2008). The development of green roof models has evolved toward increasing complexity. For example, Tabares-Velasco and Srebric (2012) set out to validate a model that computes the energy exchange between the sky, foliage, and substrate to estimate evapotranspiration, concluding a high degree of predictability for evapotranspiration, but noted predictability declined during precipitation events. During the same year, Djedjig et al. (2012) validated a heat and mass transfer model that incorporated the effects of substrate thermal inertia that was neglected in the models proposed by Alexandri and Jones (2007), Ouldboukhitine et al. (2011), Sailor (2008), and Tabares-Velasco and Srebric (2012). Although predictability of temperature and substrate moisture by the model was high, its predictions were constrained to a temporal maximum of 19 days, indicating the model may not be suitable for long-term predictions (Djedjig et al. 2012).

Recent models involved treating green roof layers as heterogeneous media (Quezada-García et al. 2017), incorporating temporal variation of traditionally fixed parameters (e.g. leaf area index (LAI) and substrate depth by He et al. (2017)), or coupling to commercial software to complement the overall analyses (e.g. TRNSYS in Lazzarin, Castellotti, and Busato (2005)). Recently, He et al. (2021) predicted hourly rates of evapotranspiration in green roofs using an array of 15 artificial neural networks, finding better predictability than vapour diffusive models. But a recent review of green roof models by Quezada-García et al. (2020) declared that there exists some merit for the development of simplified modelling approaches, as current models seemed to have been validated against variables that

are poor indicators of overall thermal performance, or have increased parameterization to simulate processes that are largely inconsequential to thermal performance.

Certainly, one approach to understanding green roof thermal performance is to characterize its thermophysical properties that regulate the energy flux occurring throughout the green roof system. Inverse modelling has proven to be of great benefit in the broader building energy simulation research field in characterizing envelope properties of existing buildings (Gunay et al. 2021), but has been largely overlooked in the green roof research space. Using inverse modelling techniques to characterize envelope properties requires a theoretical model framework, which can often be represented as a resistor-capacitor (RC) model – an electrical circuit analogy to heat transfer described in (Fraisse et al. 2002). These two techniques have been utilized not only to characterize conventional materials, but also novel ones such as phase change materials (PCMs) embedded in roof envelopes and other opaque surfaces (Elarga et al. 2017). These examples identify a unique opportunity to appeal to alternative modelling approaches in response to the declaration made by Quezada-García et al. (2020) to advance the green roof research space.

Therefore, the primary objective of this paper is to apply inverse modelling techniques to characterize the thermophysical properties of a green roof in Ottawa, Canada using a simplified RC model. Specifically, using five months' worth of measured data, we will extract the thermal resistance and capacitance of the green roof soil and canopy layers, as well as the LAI of the canopy. The secondary objective is to assess the capability of our model to predict hourly heat flux through the structural component of the green roof (concrete and insulation) and compare our results to our previous work in Gunn et al. (2021), which presents relative percent-reductions in total monthly heat exchange promoted by the green roof.

Methods

The green roof assembly consist of a 300 mm concrete slab, a rubberized asphalt waterproof roof membrane, modified bitumen sheet, 100 mm of rigid type 4 extruded polystyrene insulation (RSI = 3.52 $m^2{}^oC/W$), and a drainage mat. Above the structural component of the envelope exists ~100 mm of sandy soil and *Sedum spurium* foliage in basket-style modules. The data infrastructure of the roof includes thermocouples that have been installed at the locations indicated in Figure 1, which also includes the framework of the proposed RC model; instrumentation specifications are listed in Table 1. All data are collected in five-minute increments and has been processed into average hourly data for the analysis conducted herein.

The RC model is called by the genetic algorithm (ga) function in MATLAB which extracts the thermophysical properties listed in Table 2 during calibration, while the remaining properties are held constant. Calibration was achieved by minimizing the sum of squared differences between the modelled and measured canopy, soil, and drainage mat temperatures simultaneously over the training duration of one month. Note that the search ranges invoked by the ga function are well-defined for the soil properties, however, the properties of the canopy are less understood. As such, these search ranges are broadened over a range that captures the potential solution space of the regression analysis specific to these parameters.

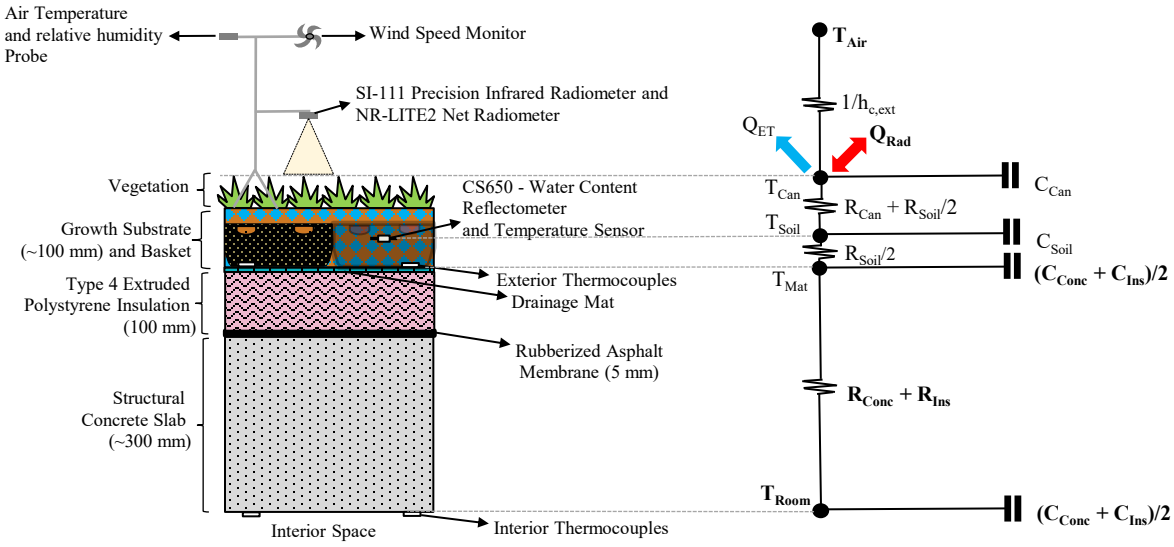

Figure 1 - Green roof instrumentation and envelope (left); Proposed RC Model framework (right); bolded terms indicate known properties or measured data.

Table 1 – Data Infrastructure Specifications

Instrument	Range	Accuracy	Precision
HC2 S3 Relative Humidity and Temperature Sensor	-50ºC to +100ºC	±0.1ºC	-
Wind Monitor	0 – 60 m/s	±0.3 m/s	-
CS650 Water Content Reflectometer and Temperature Sensor	5 – 50%	±3%	<0.05%
	-10ºC to +70ºC	±0.5ºC	±0.02ºC
Thermocouple	-	±0.2ºC	-
SI-111 – Precision Infrared Radiometer	-10ºC to +65ºC	±0.2ºC	-
NR-LITE2 Net Radiometer	-200 – 1500 W/m^2	±5%	-

Table 2 – Parameter estimate search ranges for ga function

	R_{Can}	f	C_{soil}	R_{Soil}	LAI
Units	$m^{2o}C/W$	-	$kJ/m^{2o}C$	$m^{2o}C/W$	m^2/m^2
lower	0	0	79.7	0.163	0
Upper	3	1	96.1	0.345	3

Finally, the search range of the soil thermal resistance shown in Table 2 corresponds to the lower and upper limits of the entire study period; however, for each month, these search ranges are adjusted as per the minimum and maximum monthly volumetric water contents in conjunction with the relation presented in equation 1 which was previously obtained via experiment (guarded hot plate analysis of thermal conductivity as per ASTM Standard C177), where VWC is the volumetric water content of the soil (m^3/m^3).

$$R_{soil} = \frac{0.1\ m}{1.4018 \cdot \boldsymbol{VWC} + 0.285} \quad (1)$$

The RC model consists of four transient energy balance equations, where bolded terms represent measured data or known values. The transient energy balance at the surface considers measured net radiation (Q_{Rad}), latent heat release via evapotranspiration (Q_{ET}), sensible heat exchange between the canopy surface and atmosphere via convection (Q_{conv}), and conductive heat flux between the canopy and dry soil nodes and is represented by equation 2. Convection is calculated by equation 3 which has been used to estimate sensible heat exchanges over green roof canopies in Ayata et al. (2011). Recall that LAI is the leaf area index (m^2/m^2) of the canopy.

$$C_{can}\frac{dT_{can}}{dt} = \boldsymbol{Q_{Rad}} - Q_{ET} + Q_{conv} + \frac{T_{soil} - T_{can}}{R_{can} + \frac{R_{soil}}{2}} \quad (2)$$

$$Q_{conv} = LAI \cdot h_{c,ext}(\boldsymbol{T_{air}} - T_{can}) \quad (3)$$

The exterior convection coefficient is calculated via equation 4 (McAdam's equation) and is a function of wind speed (u) and absolute air temperature (T_{air}) and is appropriate for foliage with relatively small leaf areas and wind speeds less than 5 m/s (Ayata et al. 2011). The maximum wind speed during the study period did not exceed 2.9 m/s.

$$h_{c,ext} = 5.9 + 4.1\boldsymbol{u}\left(\frac{511 + 294}{511 + \boldsymbol{T_{air}}}\right) \quad (4)$$

Latent heat exchange is quantified using the BOWEN ratio, which is defined as the ratio of sensible to latent heat exchange over bare soil or vegetative surfaces and has been used in previous green roof research in the BES tool ESP-r (Martens et al. 2008). Using the BOWEN ratio circumvents the perilous task of directly measuring latent heat exchange or estimating its magnitude based on measured data (Cascone et al. 2019), and instead forces the closure of the surface energy budget (Hu et al. 2014), which is constrained by the parameter search ranges during the calibration exercise. The BOWEN ratio is defined by equation 5:

$$\frac{Q_s}{Q_{ET}} = \gamma\frac{\Delta T}{\Delta e} \quad (5)$$

where γ is a psychometric parameter that is a function of air pressure (kPa·ºC), and ΔT and Δe are the temperature and vapour pressure gradients between the canopy surface and overlying atmosphere, respectively. The vapour pressure at the canopy surface is assumed to be saturated and Δe is computed using relative humidity data measured above the green roof and an empirical relation described by Dingman (2015). Hence, we present an expanded form of the transient energy balance at the surface shown by equation 6. Finally, we note that the thermal capacitance of the canopy is estimated via equation 7, which treats the canopy layer as a heterogeneous layer comprised of both plant matter and air.

$$C_{can}\frac{dT_{can}}{dt} = \boldsymbol{Q_{Rad}} - \left[\frac{LAI \cdot h_{c,ext}(\boldsymbol{T_{air}} - T_{can})}{\gamma\frac{(T_{can} - \boldsymbol{T_{air}})}{(e_{sat} - e_{air})}}\right] + \left[LAI \cdot h_{c,ext}(\boldsymbol{T_{air}} - T_{can})\right] + \frac{T_{soil} - T_{can}}{R_{can} + \frac{R_{soil}}{2}} \quad (6)$$

$$C_{can} = f(\boldsymbol{\rho C_p})_{plants}\boldsymbol{d_{can}} + (1 - f)(\boldsymbol{\rho C_p})_{air}\boldsymbol{d_{can}} \quad (7)$$

where C_{can} is the estimated thermal capacitance of the canopy layer (J/m^{2o}C), ρ_{plants} and $C_{p,plants}$ are the density (582 kg/m^3) and specific heat capacity (4800 J/kgºC) of the plants; ρ_{air} and $C_{p,air}$ are the density (1.184 kg/m^3) and specific heat capacity (1007 J/kgºC) of the air (Polo-Labarrios et al. 2020); d_{can} is the assumed height of the canopy layer (0.05 m), and f is the volumetric fraction of the

foliage within the canopy layer. The transient energy balance at the soil node is provided by equation 8. The storage term considers both the thermal capacitance of the soil (C_{soil}) and water (C_w) held therein. The thermal capacitance of the water is computed by equation 9, where ρ_w is the density of water (1000 kg/m^3), $C_{p,w}$ is the specific heat capacity of liquid water (4184 J/kg·^{o}C), and d_{soil} is the thickness of the soil layer (m). The dry soil VWC is measured with time using the CS650 sensor shown in Figure 1.

$$(C_{soil} + \boldsymbol{C_w})\frac{dT_{soil}}{dt} = \frac{T_{can} - T_{soil}}{R_{can} + \frac{R_{soil}}{2}} + \frac{T_{mat} - T_{soil}}{\frac{R_{soil}}{2}} \quad (8)$$

$$\boldsymbol{C_w} = \boldsymbol{\rho_w C_{p.w} d_{soil}} \times \boldsymbol{VWC} \quad (9)$$

The transient energy balance at the drainage mat is represented by equation 10 and equation 11 considers heat flux through the structural portion of the green roof envelope. The thermal resistance and capacitance of concrete and insulation are 0.5 m^{2o}C/W, 43.9 kJ/m^{2o}C, 3.52 m^{2o}C/W, and 5.85 kJ/m^{2o}C, respectively. The distribution of thermal capacitance is consistent with how EnergyPlus assigns thermal mass to roofs (DOE 2020).

$$\frac{1}{2}(\boldsymbol{C_{conc}} + \boldsymbol{C_{ins}})\frac{dT_{mat}}{dt} = \frac{T_{soil} - T_{mat}}{\frac{R_{soil}}{2}} + \frac{\boldsymbol{T_{room}} - T_{mat}}{\boldsymbol{R_{ins}} + \boldsymbol{R_{conc}}} \quad (10)$$

$$\frac{1}{2}(\boldsymbol{C_{conc}} + \boldsymbol{C_{ins}})\frac{d\boldsymbol{T_{room}}}{dt} = \frac{\boldsymbol{T_{room}} - T_{mat}}{\boldsymbol{R_{ins}} + \boldsymbol{R_{conc}}} \quad (11)$$

Results

Table 3 shows the extracted monthly thermal properties of the soil and canopy layers of the green roof per square meter of green roof surface. All the estimated parameters fall within the search ranges invoked by the ga function except canopy and soil resistance (August and September, respectively), which were returned as the lower bounds of the search ranges.

Notably, canopy resistance did not significantly contribute to the total thermal resistance of the green roof. However, the thermal capacitance of the canopy layer remained above 108 kJ/m^{2o}C over the study period, which was higher than that of dry soil each month, which ranged between 91.9 – 95.7 kJ/m^{2o}C. Note, however, soil moisture accounts for a considerable amount of thermal mass in the soil, which ranged between 1.4 and 97.8 kJ/m^{2o}C and was explicitly calculated in the model via equation 9.

Despite the high heat storage of the canopy, we note that water storage in foliage can be as high as 90% by mass (Jones 2013), and previous green roof models have assumed canopy heat capacity was equal to that of water at 4184 J/kg^{o}C (Arkar et al. 2018). The thermal resistance of the soil tended be skewed toward the lower bound of the search range for every month of the study period, and LAI tended lower than one for each month, which is atypical for most forms of extensive green roof foliage (Zhou et al. 2018).

The canopy surface in the proposed RC model plays a significant role in regulating energy fluxes throughout the roof assembly by partitioning the incoming short and longwave radiation into its constituent sensible, conductive, and latent energy components. Figure 2 illustrates the energy partitioning at the canopy surface during of July 2016, where it is evident that a substantial portion of incoming net radiation is converted latent energy due to effects of evapotranspiration.

Indeed, application of the BOWEN ratio indicates the main cooling mechanism at the green roof surface is due to evapotranspiration, the behaviour of which appeared inversely proportional to net radiation measurements, with minimal latent heat release occurring during rainfall events and times of high relative humidity by virtue of a decreased vapour pressure gradient above the roof. Convection played a less important role in both heating and cooling of the canopy surface. This result is consistent with measured wind speed above the green roof, which had a mean value of 0.51 m/s over the entire study period and did not exceed 2.86 m/s. The predicted temperatures returned by the proposed RC model appear to follow an overall similar behaviour to the measured values, with most discrepancy occurring at the canopy as illustrated in Figure 3 and as indicated by the RMSE values reported in Table 3, which were greatest for the predicted canopy temperature over every month of the study period.

Table 3 – Estimated thermophysical properties of green roof soil and canopy layers with optimization metrics

Param.	**R_{Can}**	**C_{can} (*f*)**	**C_{Soil}**	**C_w**	**R_{Soil}**	**LAI**	**RMSE T_{Can}**	**RMSE T_{Soil}**	**RMSE T_{Mat}**
Month	*(m^{2o}C/W)*	*(kJ/m^{2o}C)*	*(kJ/m^{2o}C)*	*(kJ/m^{2o}C)*	*(m^{2o}C/W)*	*(m^2/m^2)*	*(^{o}C)*	*(^{o}C)*	*(^{o}C)*
May	0.0127	137 (*0.98*)	95.7	4.3 – 61.4	0.209	0.65	5.87	3.33	3.22
June	0.0004	138 (*0.99*)	95	2.1 – 52.3	0.224	0.564	6.26	3.79	3.37
July	0.0394	112 (*0.80*)	93.7	11.7 – 77.3	0.205	0.644	5.2	2.11	2.23
August	0	112 (*0.80*)	92.4	1.4 – 82.0	0.179	0.526	5.02	3.18	2.55
September	0.0168	108 (*0.78*)	91.9	21.1 – 97.8	0.176	0.551	3.46	1.76	1.76

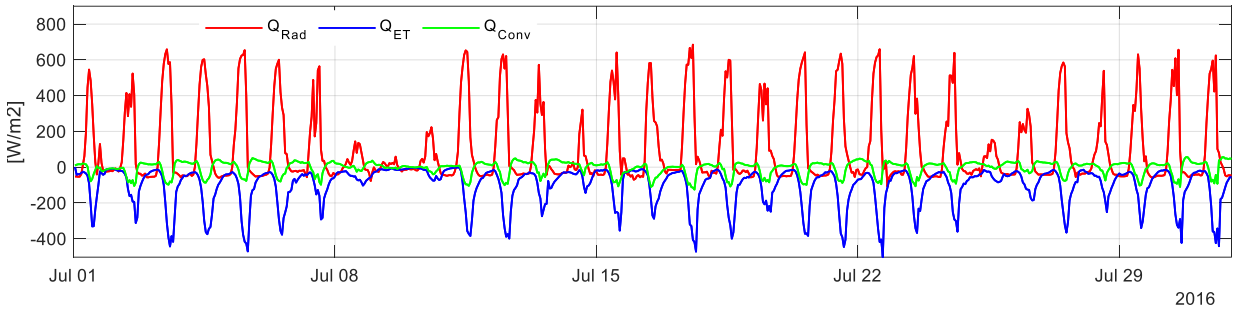

Figure 2 – Surface energy fluxes predicted by the proposed RC model for the month of July 2016.

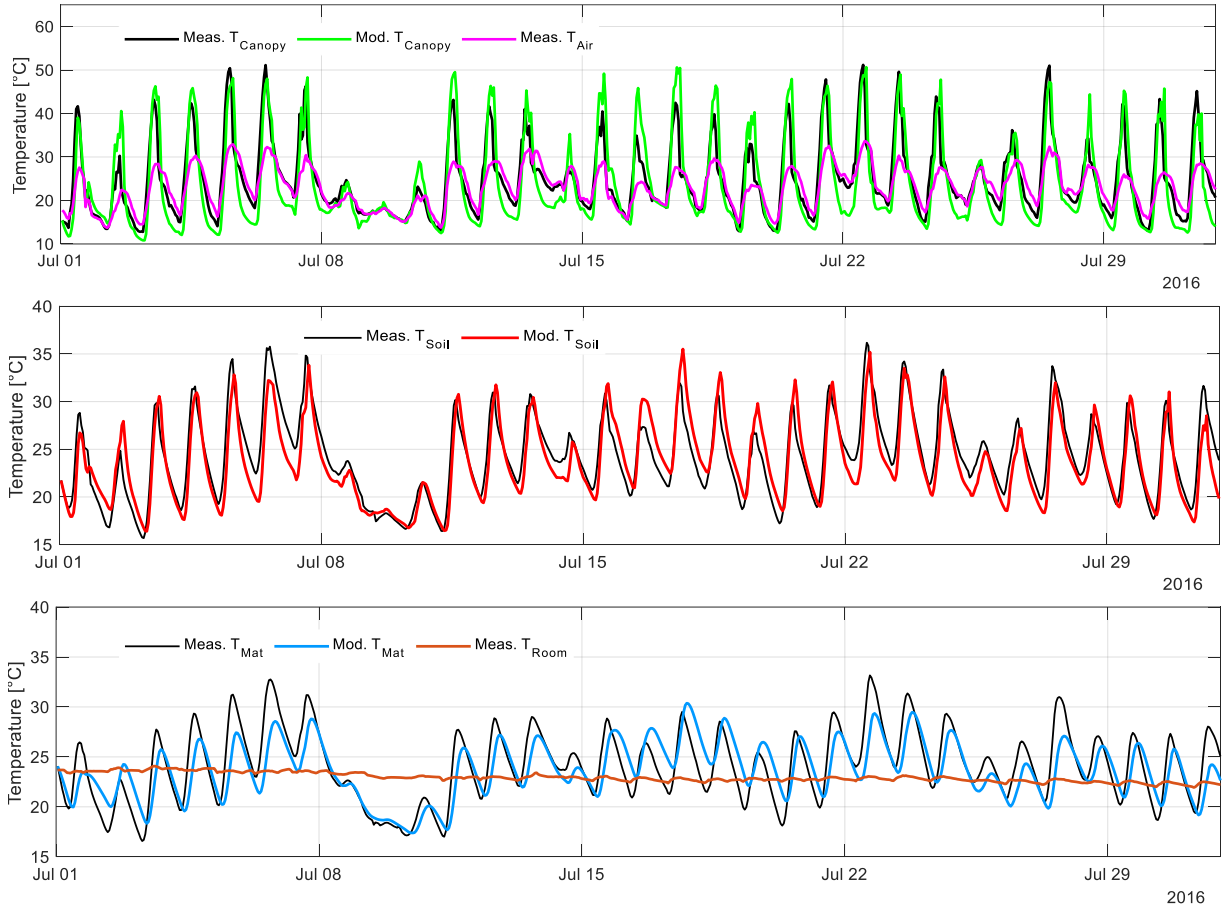

Figure 3 – Top) meas. and mod. canopy temperature and air temperature 1.5 m above green roof; middle) meas. and mod. soil temperature; bottom) meas. and mod. drainage mat temperature, and meas. room temperature.

The proposed RC model exhibits difficulty in predicting canopy temperatures during the night, when canopy and ambient air temperatures were nearly identical; hence, convective heat exchange during the night tends to be overestimated in magnitude via equations 3 and 4. Conversely, predicted drainage mat temperatures tend to exhibit less variation than the measured data, which may be attributed to the thermal mass governing the incremental variation of that temperature during each timestep as illustrated by equation 10.

Discussion

Previous work by the authors quantified percent reductions of total heat exchange promoted by the green roof relative to a conventional roof (Gunn et al. 2021). In this paper, our secondary objective was to evaluate the capability of the proposed RC model to simulate heat flux through the structural component of the green roof and investigate how these simulated fluxes translate into discrepancies between measured and modelled green roof thermal performance per month. Figure 4 shows the measured and predicted hourly heat flux (q_{roof}) through the structural portion of the green roof in July compared to measured heat flux on the

conventional roof. During the first week of July in Figure 3, modelled canopy temperatures at their mid-day peak fall below measured values slightly; this effect is exhibited at the soil and mat nodes and is amplified at successive depths. This result may be due to the relatively high heat storage in the canopy, which was found to be comparable to that of moist soil (Table 3). Indeed, more heat storage at the canopy results in less heat available for transmission through the soil and underlying layers. This could also be why the thermal resistance of the soil was near the lower boundary of its search range each month, as noted previously. We also observe a distinct trade-off between the availability of transmitted heat from above to the drainage mat and the thermal capacitance assigned to the drainage mat node in the model. For example, the dampened oscillation in modelled mat temperature is regulated by the amount of thermal mass assigned to the mat node in the model, which is based on known material properties of concrete and insulation. Therefore, the assigned thermal mass at the drainage mat may simply not allow for the observed temperature variation that is measured. Overall, the model predicts hourly heat flux over the entire study period with a maximum error of 0.838 W/m^2 as reported in Table 4, which also shows the measured total heat exchange through the green and conventional roofs, as well as predicted total heat exchange through the green roof and relative percent reductions in total heat exchange.

Considering Table 4, we note that the predicted percent reductions in total heat exchange are similar to the measured percentages during the shoulder seasons (May and September) but tend to be overestimated during the hotter summer months. It is unclear why this discrepancy occurs, but we note that a larger fraction of the total flux through the roof during May and September is heat loss (89.7% and 84.3%, respectively), when modelled mat temperature is less dependent on heat transfer through the vegetation and canopy, the properties of which are reliant on the calibration process.

Notably, the predicted percent reduction in June exhibits the greatest discrepancy (17.2%) from the measured percentage, when the net heat exchange over the month was closer to 0 kWh/m^2 than any other month in the study period. Figure 5 demonstrates that hourly heat flux is better predicted when dividing the calibration process during June into two separate training regimes (June 1, 12:00 AM – June 15, 1:00 PM and June 15, 1:00 PM – June 30, 12:00 AM). Table 5 shows the parameters and performance metrics associated with the two separate simulations, and that the modelled relative percent reductions in total heat exchange are improved by 11.4% and 4.8% for simulations 1 and 2, respectively. This result indicates the model training duration may be limited to less than 720 data points for June.

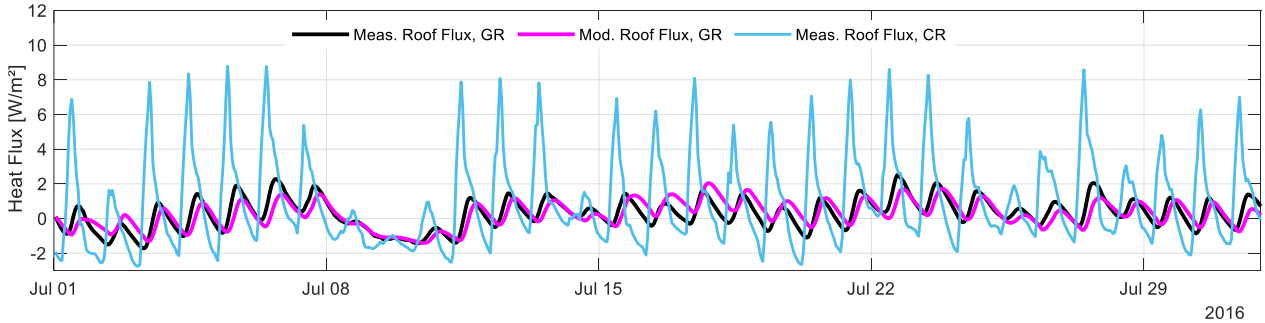

Figure 4– Measured and predicted heat flux, q_{roof}, through structural portion of the green roof (concrete and insulation); measured heat flux through conventional roof; positive values indicate downward heat flux into the room.

Table 4 – RMSE of modelled hourly heat flux, q, through structural component of green roof, and total monthly heat exchanges, q_{tot}, through green and conventional roofs. "GR" indicates green roof and "CR" indicates conventional roof.

Month	**RMSE**	**Total Heat Exchange, $q_{roof,tot}$**			**Percent Reduction in Total Heat Exchange**	
		Measured, GR	Modelled, GR	Measured, CR		
	(W/m^2)	*(kWh/m^2)*	*(kWh/m^2)*	*(kWh/m^2)*	*Measured*	*Modelled*
May	0.801	1.001	1.027	1.824	45.1%	43.7%
Jun	0.838	0.722	0.462	1.516	52.3%	69.5%
Jul	0.554	0.552	0.440	1.469	62.4%	70.1%
Aug	0.634	0.597	0.487	1.349	55.7%	63.9%
Sep	0.437	0.689	0.663	1.217	43.4%	45.6%

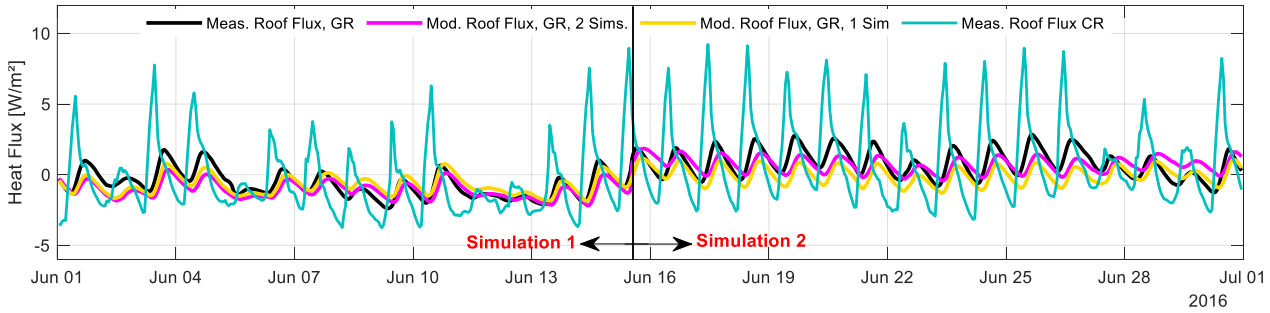

Figure 4 – June 2016, comparison of measured and predicted hourly heat flux, q_{roof}, through structural portion of green roof for single and 2 separate simulations. Conventional roof heat flux for reference.

Table 5 - June 2016 - Parameters and performances indicators for simulations 1 and 2

	Sim. 1	**Sim. 2**
R_{Can} (m^2°C/W)	0.0126	0.0232
C_{Can} (f) (kJ/m^2°C)	135 (0.97)	129 (0.92)
C_{Soil} (kJ/m^2°C)	93613	82214
R_{Soil} (m^2°C/W)	0.220	0.288
LAI (m^2/m^2)	0.794	0.462
RMSE T_{Can} (°C)	4.92	7.17
RMSE T_{Soil} (°C)	3.05	3.70
RMSE T_{Mat} (°C)	2.91	3.40
RMSE q_{roof} (W/m^2)	0.723	0.847
$q_{roof,tot}$ GR (kWh/m^2)	345.3	377.1
$q_{roof,tot}$ GR (kWh/m^2)	384.7	274.8
$q_{roof,tot}$ CR (kWh/m^2)	685.9	830.1
Meas. % Reduction	49.7%	54.6%
Mod. % Reduction	43.9%	66.9%

Conclusions

In this paper, we implemented a simplified RC model to characterize the thermal performance of a green roof using inverse modelling techniques. The model's performance was investigated with five months of data from a green roof in Ottawa, Canada. Estimated dry soil thermal capacitances and resistances were similar during each month at averages of 93.8 kJ/m^2°C and 0.198 m^2°C/W, respectively. Canopy thermal capacitance played a significant role in heat storage at the surface, ranging between 108 – 138 kJ/m^2°C, while canopy resistance appeared to have a negligible impact on total thermal transmittance. LAI did not follow any discernible trend, and retroactive assessment of foliage condition was not possible at the time of writing this paper. Simulated canopy temperature exhibited the greatest RMSE of 5.16°C on average across all months, which was 1.82 and 1.97 times greater than the 5-month average RMSE of simulated soil and mat temperatures, respectively. The RC model exhibited difficulty simulating heat flux through the structural portion of the roof during months when hourly flux was mainly positive, which translated into overestimated relative percent reductions in total heat exchange by a maximum of 17.2% (June). However, separating the calibration process in June into 2 timeframes yielded improved predictability of relative performance, indicating some temporal limitation on simulation time. To build on this research, an implicit finite difference model for the same roof assembly will be developed and subject to the same analysis, which may produce more accurate predictions of mat temperature and thus heat flux which was restricted in this study due to the spatial coarseness of the RC model configuration.

References

Alexandri, E. and P. Jones (2007). Developing a One-Dimensional Heat and Mass Transfer Algorithm for Describing the Effect of Green Roofs on the Built Environment: Comparison with Experimental Results. *Building and Environment 42* (8): 2835–49.

Arkar, C., S. Domjan, and S. Medved. (2018). Heat Transfer in a Lightweight Extensive Green Roof under Water-Freezing Conditions. *Energy and Buildings 167* (May): 187–99.

Ayata, T., P. Tabares-Velasco, and J. Srebric (2011). An Investigation of Sensible Heat Fluxes at a Green Roof in a Laboratory Setup. *Building and Environment 46* (9): 1851–61.

Boafo, F. E., J-T. Kim, and J-H. Kim (2017). Evaluating the Impact of Green Roof Evapotranspiration on Annual Building Energy Performance. *International Journal of Green Energy 14* (5): 479–89.

Burak, H. B., D. Darwazeh, S. Shillinglaw, and I. Wilton (2021). Remote Characterization of Envelope Performance through Inverse Modelling with Building Automation System Data. *Energy and Buildings 240*: 110893.

Cascone, S., J. Coma, A. Gagliano, and G. Pérez (2019). The Evapotranspiration Process in Green Roofs: A Review. *Building and Environment 147* (October 2018): 337–55.

Department of Energy (2020). Engineering Reference - EnergyPlus Documentation.

Dingman, S. L. (2015). *Physical Hydrolgoy*. Prentice Hall. Upper Saddle River (US)

Djedjig, R., S-E Ouldboukhitine, R. Belarbi, and E. Bozonnet. (2012). Development and Validation of a

Coupled Heat and Mass Transfer Model for Green Roofs. *International Communications in Heat and Mass Transfer* 39 (6): 752–61..

Elarga, H., S. Fantucci, V. Serra, R. Zecchin, and E. Benini. (2017). Experimental and Numerical Analyses on Thermal Performance of Different Typologies of PCMs Integrated in the Roof Space. *Energy and Buildings* 150: 546–57.

Fraisse, G., C. Viardot, O. Lafabrie, and G. Achard (2002). Development of a Simplified and Accurate Building Model Based on Electrical Analogy. *Energy and Buildings* 34 (10): 1017–31.

Francis, R. A., and J. Lorimer (2011). Urban Reconciliation Ecology: The Potential of Living Roofs and Walls. *Journal of Environmental Management* 92 (6): 1429–37.

Gunn, P., H. B. Gunay, and P. J. van Geel (2021). A Multi-Year Comparative Analysis of Green and Conventional Roof Thermal Performance under Temperate Climate Conditions. *Proceedings from 8th International Building Physics Conference*. Copenhagen (Denmark), 25-27 August 2021.

He, Y., E. S. Lin, C. L. Tan, P. Y. Tan, and N. H. Wong (2021). Quantitative Evaluation of Plant Evapotranspiration Effect for Green Roof in Tropical Area: A Case Study in Singapore. *Energy and Buildings 241*: 110973.

He, Y., H. Yu, A. Ozaki, N. Dong, and S. Zheng (2017). Influence of Plant and Soil Layer on Energy Balance and Thermal Performance of Green Roof System. *Energy 141*: 1285–99.

Hu, S., C. Zhao, J. Li, F. Wang, and Y. Chen (2014). Discussion and Reassessment of the Method Used for Accepting or Rejecting Data Observed by a Bowen Ratio System. *Hydrological Processes 28* (15): 4506–10.

Jones, H. G. (2013). *Plants and Microclimate: A Quantitative Approach to Environmental Plant Physiology*. *Plants and Microclimate: A Quantitative Approach to Environmental Plant Physiology*. Cambridge UniveRty Press. Cambridge (UK)

Lazzarin, R. M., F. Castellotti, and F. Busato (2005). Experimental Measurements and Numerical Modelling of a Green Roof. *Energy and Buildings 37* (12): 1260–67.

Martens, R., B. Bass, and S. S. Alcazar (2008). Roof-Envelope Ratio Impact on Green Roof Energy Performance. *Urban Ecosystems 11* (4): 399–408.

Ouldboukhitine, S. E., R. Belarbi, I. Jaffal, and A. Trabelsi (2011). Assessment of Green Roof Thermal Behavior: A Coupled Heat and Mass Transfer Model. *Building and Environment 46* (12): 2624–31.

Polo-Labarrios, M. A., S. Quezada-Garciá, H. Sánchez-Mora, M. A. Escobedo-Izquierdo, and G. Espinosa-Paredes (2020). Comparison of Thermal Performance between Green Roofs and Conventional Roofs. *Case Studies in Thermal Engineering 21* (November 2019).

Quezada-García, S., G. Espinosa-Paredes, M. A. Escobedo-Izquierdo, A. Vázquez-Rodríguez, R. Vázquez-Rodríguez, and J. J. Ambriz-García (2017). Heterogeneous Model for Heat Transfer in Green Roof Systems. *Energy and Buildings 139*: 205–13.

Quezada-García, S., G. Espinosa-Paredes, M. A. Polo-Labarrios, E. G. Espinosa-Martínez, and M. A. Escobedo-Izquierdo (2020). Green Roof Heat and Mass Transfer Mathematical Models: A Review. *Building and Environment 170* (December 2019): 106634.

Saadatian, O., K. Sopian, E. Salleh, C. H. Lim, S. Riffat, E. Saadatian, A. Toudeshki, and M.Y. Sulaiman (2013). A Review of Energy Aspects of Green Roofs. *Renewable and Sustainable Energy Reviews 23*: 155–68.

Sailor, D. J. (2008). A Green Roof Model for Building Energy Simulation Programs. *Energy and Buildings 40* (8): 1466–78.

Santamouris, M.(2014). Cooling the Cities - A Review of Reflective and Green Roof Mitigation Technologies to Fight Heat Island and Improve Comfort in Urban Environments. *Solar Energy 103*: 682–703.

Susca, T. (2019). Green Roofs to Reduce Building Energy Use? A Review on Key Structural Factors of Green Roofs and Their Effects on Urban Climate. *Building and Environment 162* (March): 106273.

Tabares-Velasco, P. C., and J. Srebric (2012). A Heat Transfer Model for Assessment of Plant Based Roofing Systems in Summer Conditions. *Building and Environment 49* (1): 310–23.

Talebi, A., S. Bagg, B. E. Sleep, and D. M. O'Carroll (2019). Water Retention Performance of Green Roof Technology: A Comparison of Canadian Climates. *Ecological Engineering 126* (May 2018): 1–15.

Zhou, L. W., Q. Wang, Y. Li, M. Liu, and R. Z. Wang. (2018). Green Roof Simulation with a Seasonally Variable Leaf Area Index. *Energy and Buildings 174*: 156–67.